

CMOS Silicon Photomultiplier Development

N. D'Ascenzo, V. Saveliev and Q. Xie

Abstract CMOS - complementary metal-oxide-semiconductor technology at present time is the most advanced and popular semiconductor technology for the development and production of microelectronic elements. Many signs have long pointed toward CMOS as the preferable sensor technology of the future. In many ways, the bright future for CMOS sensor technology was made officially by leading electronic companies in early 2015 to claim that up to 2025 all kind of sensors will be produced in CMOS technology. Beyond this, improvements to CMOS technology and the strong price/performance ratio of CMOS sensors make them increasingly attractive for many academic and industrial applications. The development of Silicon Photomultiplier (SiPM) - a new sensor for the low photon flux in standard CMOS technology - is an important new step for the development, optimisation and mass production of SiPM for the wide application areas as nuclear medicine, experimental physics, visualisation systems. It is an important step for the future developments of new SiPM structures, especially advanced digital SiPM structures, digital SiPM imagers, and avalanche Pixel structures for the detection of ionisation particles.

1 Introduction

For more than 60 years Photomultiplier Tubes (PMTs) have been filling the area of detection of low photon flux practically without alternative [1], despite the fact that the many critical fundamental disadvantages of this devices are very well known.

N. D'Ascenzo

Huazhong University of Science and Technology, Wuhan China e-mail: ndasc@hust.edu.cn

V. Saveliev

Huazhong University of Science and Technology, Wuhan China e-mail: saveliev@hust.edu.cn

Q. Xie

Huazhong University of Science and Technology, Wuhan China e-mail: qgxie@hust.edu.cn

Concerning modern semiconductor structures for the low photon flux detection, few options were investigated, but the main critical problem to develop the semiconductor device for the extremely low photon flux was the relative high level of thermal noise of the semiconductor detector structures and the associated front-end electronics. The solution of this problem can be done in two ways: cooling the photosensor and the related front-end electronics or providing a very high value of intrinsic amplification, up to 10^6 , as comparable to the PMT.

One of the solutions to overcome the noise problem is the Visible Light Photon Counter (VLPC) [2]. This photosensor is realized as a semiconductor avalanche structure operated at the temperature of 4K, for the suppression of thermal noise. The results were successful and showed the possibility to detect low photon flux up to a single photon. However the operational conditions were too complicated to be acceptable for a wide area application as this sensor needed to be operated a cryostat down to a temperature of 4K. This is up to now a challenge even in laboratory conditions.

The development of the modern detection structures for the low photon flux, known at present time as Silicon Photomultiplier, was initiated at the beginning of the '90s, starting with the study of Silicon Metal Oxide Semiconductor (MOS) structures with avalanche breakdown mode operation for the detection of single photons. The results were positive, but the strong limitation was the necessity to include external recharge circuits for the discharge of the sensor structure after charging the MOS structure during the photons detection.

The next step was the implementation of a special resistive layer instead of oxide layers. These so-called Metal Resistive Semiconductor (MRS) structures gave the possibility to recharge the structure after photon detection and in addition to control the breakdown avalanche process by quenching. Such structures had very high and stable amplification suitable for single photons detection, in comparison to conventional avalanche photodetector structures, but limited sensitive area.

The idea of Silicon Photomultiplier or more precisely Silicon Photoelectron Multipliers was created to overcome the problem of the above mentioned structures as small sensitive area due to the instability of amplification over large area, low dynamic range and slow response.

It was decided to create semiconductor structures consisting of space distributed fine metal resistor semiconductor micro sensors with individual quenching and common output. The result was impressive: for the first time a clear single photon spectra was detected on the semiconductor structure at room temperature with high resolution.

The first concept of Silicon Photomultiplier was proposed as fine silicon structure of avalanche breakdown mode micro-cells with common resistive layer, quenching element and common electrodes [3].

The goals of the next steps in the development of the Silicon Photomultiplier were the optimization of the detection structures, in particular increasing the so-called geometrical efficiency. This quantity consists of the ratio of the photon-sensitive-area to the total area of the silicon photomultiplier. Its increase allows for getting an higher detection efficiency. Further optimization goals were the tun-

ing of the optimal operation condition in terms of bias and time performance, and generally the improvement of the technological processes.

With the advanced technology, that became available in the middle of the '90s, the micro-cells were positioned as close as possible to each other, the common resistive layer as quenching element was substituted by individual integrated resistors coupled to the individual micro-cells with optimization of position and size. In this way the modern silicon photomultiplier structures start to be available for the applications [4].

The new problem of the optimized structures of silicon photomultipliers was the optical crosstalk in fine detection structure due to light emission during the avalanche breakdown processes in Silicon. The phenomena of light emission from avalanche breakdown process is well known [5]. In the Silicon Photomultipliers with tiny space structure of microcells, the probability of detection of secondary photons by neighbourhood microcells is quite high and should be taken into account. Mainly this problem is affecting the area of very low photon flux detection, where the optics crosstalk could significantly change the results of the measurement. The solution of this problem was achieved by the implementation of modern technology processes, the physically optical isolation of the micro-cells on the integrated structure level. For the suppression of the optical crosstalk between the micro-cells, the trench structure was implemented around micro-cells as optic isolating elements and filled by optic non transparent material. The latest development in this area brings the very high performance for very low photon flux and created a special type of silicon photomultiplier - quantum photo detectors (QPD) [6].

The Silicon Photomultiplier is the first semiconductor detector, which not only could compete with photomultiplier tubes in term of detecting of low photon flux, but has great advantages in performance and operation conditions and has great future in many areas of applications such as experimental physics, nuclear medicine, homeland security, military applications and other. Silicon Photomultipliers show an excellent performance including the single photon response at room temperature (intrinsic gain of multiplication is 10^6), high detection efficiency 25-60 % for the visible range of light, fast timing response 30 ps. Operational conditions are suitable for many applications: operation bias 20-60 V, operated at room temperature as well in cooling conditions, not sensitivity to electromagnetic fields. The production on the basis of modern semiconductor technology, compatible with mass production semiconductor technology, compact, typical size of few mm^2 and flexible for assembling of the arrays. In this publication is impossible to explore all aspects of the Silicon Photomultiplier discovery and we will mainly emphasise the more common features of the silicon photomultiplier development.

In the same time all developments of the SiPM is done on the basis of a special semiconductor technology, which actually is not necessary. The semiconductor material for the SiPM does not require the special characteristic as high resistivity, or high purity and can be produced using standard CMOS technology materials. This feature opens the way to use the modern advanced technology as CMOS technology for the production of the conventional SiPMs and speeds up the progress of the future development of SiPM, especially of the Digital Silicon Photomultiplier which

combine the sensors with the modern processing electronic on the same substrate and generally use the all modern development in microelectronic area [7, 8, 9, 10].

2 The CMOS Silicon Photomultiplier Technology

A detailed description of the Silicon Photomultiplier structure and operational principle can be found in [11, 12, 13]. In this chapter we focus on the improvement and optimization of the performances of Silicon Photomultipliers by using standard CMOS technology [14, 15]. This topic has currently a strong research interest.

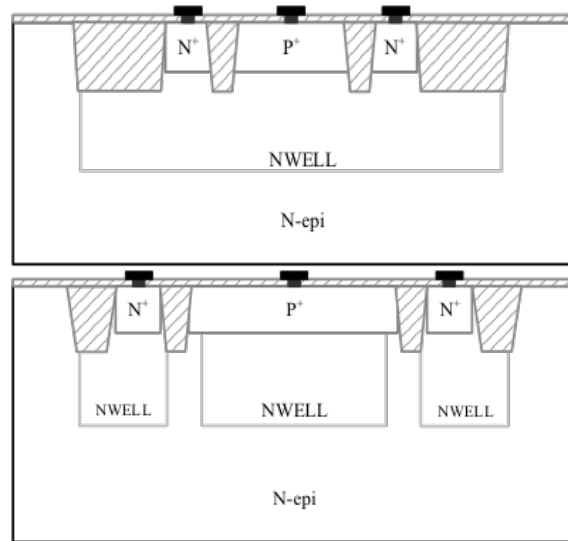


Fig. 1 Cross section of the CMOS SiPM detection structures. STI guard ring (up) and Virtual guard Ring (down).

Few not trivial issues are faced in the design of SiPM in standard CMOS technology. First the achievement of the proper breakdown condition corresponding to an electric field configuration localized mainly in the breakdown region itself. Second the design of highly resistive quenching element integrated within the cell, guaranteeing small thickness, small size, precision at the level of few %. Third the uniform spread of the electric field along the junction, avoiding premature breakdown on the edges of the junction.

However, SiPM can suffer of localised breakdown conditions on the locally concentrated high electric field at the junction edges. The use of guard ring structures around the sensitive area of each microcell is in this respect mandatory in order to obtain a uniform electric field across the whole sensitive area. The CMOS technology offers few possibilities of implementing such guard rings [16, 14, 15, 17, 24].

Among the others, two detection structures possible within standard CMOS processes are proposed in this chapter. The SiPM detection structure shown in Fig. 1(up) has shallow trench isolation (STI) guard ring. The SiPM detection structure shown in Fig. 1(down) has a virtual guard ring. In the second structure STI are formed close to the p^+ implantation as a standard procedure in the CMOS process, but kept far from the sensing area of the photo-detector.

The structures are operated in breakdown mode and a quenching element is needed in order to stop the avalanche. A passive quenching element consists of a resistor integrated around the sensitive cell. The standard CMOS technology processes include High Resistive Polysilicon as a standard option.

3 Mathematical modelling of the CMOS Silicon Photomultiplier

The mathematical modelling of the CMOS Silicon Photomultiplier detection structure plays a central role in the design of the photodetector. Following the recent trends in CMOS sensor design, in fact, a mathematical model with strong predictive power offers a guidance in the choice of the technology processes minimising the risks and the costs of a less efficient trial-and-error procedure.

With respect to other photodetectors, the CMOS Silicon Photomultiplier is fabricated using standard processes, whose theoretical understanding and simulation are well-established due to their large use in the manufacturing of electronics components. On this basis the key-problem in the modelling of the CMOS Silicon Photomultiplier is the correct reproduction of the conditions of the avalanche-breakdown process, which are very sensitive to the correct computation of the electron-holes currents and of the electric field corresponding to the applied external bias. A predictive calculation requires a precision of few millivolts in correspondence to a current of few microamperes and an internal detection structure electric field of about 10^5 V/cm within few microns. Such precision goes well ahead the standard requirements of electronic components simulation, as transistors or common diodes, and is based on a correct selection of a list of reasonable physical processes as well as on a robust numerical algorithm.

The task of the mathematical modelling consist of the estimation of the electric field structure corresponding to the technological parameters and geometry of the sensor. Finally the mathematical model should provide a set of observables, which could be measured in a dedicated experimental set-up and help the guidance of the technological choices.

3.1 *Physics processes*

The physics processes involved in the condition of avalanche-breakdown identify a typical coupled problem, in which the conservation of the number and energy of

electrons and holes should satisfy the additional constrain of the strong electric field generation, when an external bias is applied to the structure.

The relation of the electrostatic potential to the space charge density is described by the Poisson's Equation:

$$\nabla(\epsilon\nabla\phi) = -\rho \quad (1)$$

where:

ρ is the local space charge density

ϕ is the electrostatic potential

ϵ is the local permittivity

The electric field \mathbf{E} is defined from the electrostatic potential as $\mathbf{E} = -\nabla\phi$.

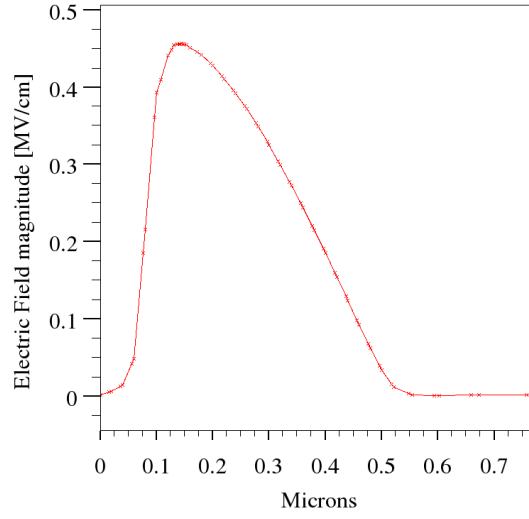


Fig. 2 1-dimensional profile of the electric field obtained on a typical CMOS SiPM detection structure.

The continuity equations for electrons and holes are defined by the equations:

$$\frac{\partial n}{\partial t} = \frac{1}{q} \nabla \cdot \mathbf{J}_n + G_n - R_n \quad (2)$$

$$\frac{\partial p}{\partial t} = -\frac{1}{q} \nabla \cdot \mathbf{J}_p + G_p - R_p \quad (3)$$

where:

n is the electron concentration

p is the holes concentration

\mathbf{J}_n is the electron current density

\mathbf{J}_p is the holes current density

- G_n is the generation rate for electrons
- G_p is the generation rate for holes
- R_n is the recombination rate for electrons
- R_p is the recombination rate for holes
- q is the electric charge of an electron

The generation rate $G_{n,p}$ for electrons and holes plays a central role in the correct physical modelling of the SiPM detection structure. When the electric field is strong enough, typically stronger than 10^5 V/cm, free carriers are accelerated, reach an energy higher than the ionization energy for electrons and holes and generate more free carriers in collisions with the atoms of the crystals. Such process is called impact ionization.

The 1-dimensional profile of the electric field corresponding to a typical CMOS SiPM detection structure is shown on Fig. 2, calculated using Eq. 1, is shown on Fig. 2. The electric field reaches a maximal value of approximately 4.4×10^5 V/cm within the junction.

The impact ionization process is described by the impact ionization of electrons and holes, respectively α_n and α_p , as:

$$G_{n,p} = \alpha_{n,p} \mathbf{J}_{n,p} \quad (4)$$

The ionization coefficient represents the number of electron-hole pairs generated by each carrier per unit distance. The correct evaluation of this parameter and its experimental validation is by far the most important part of the simulation of the CMOS Silicon photomultiplier. The estimation of the breakdown voltage, of the working current and of the response of the photodetector depends on the value of the impact ionization parameter. We find that the temperature dependent Toyabe impact ionization model is more precise and realistic for the estimation of the ionization rate in the sensitive areas of the Silicon Photomultiplier detection structure [18].

The recombination rate $R_{n,p}$ for electrons and holes is calculated according with the Shockley-Read-Hall [19] and three particle transition Auger models [20] and describes the phonon transition in the presence of a trap within the forbidden gap of the semiconductor.

The mathematical model allows for separating the contribution of the different processes to the total current. On Fig. 3 the total current corresponding to a typical CMOS SiPM detection structure and the study of the different contributions is shown. The full dots represent the total current. The separated components correspond to the recombination (Auger and Shockley-Read-Hall) and the impact ionization processes. An additional line on the plot corresponds to a physical model without the impact ionization process. Up to approximately 8 V the recombination current from Auger and Shockley-Read-Hall is dominant. At around 8 V the electric field strength is high enough for a significant contribution of the impact ionization process, which becomes clearly dominant at the breakdown. We observe that at breakdown the recombination current has a drop. The curve corresponding to the physical model without impact ionization shows that the recombination current is by far the leading current above the breakdown voltage and determines the dark

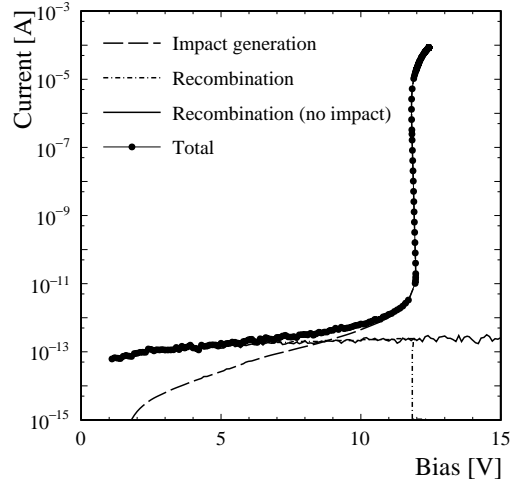


Fig. 3 Separation of the current contributions corresponding to the recombination (Auger and Shockley-Read-Hall) and the impact ionisation processes in the mathematical modelling of a typical CMOS SiPM detection structure.

current level of the CMOS SiPM detector when an avalanche is not triggered by a photon or a thermal electron-hole pair.

An additional equation is needed for the estimation of the carriers temperature. We use the energy balance transport model consisting of the equations for electrons and holes:

$$\nabla \cdot \mathbf{S}_n = \frac{1}{q} \mathbf{J}_n \cdot \mathbf{E} - W_n - \frac{3k}{2} \frac{\partial}{\partial t} \lambda_n n T_n \quad (5)$$

$$\mathbf{J}_n = q D_n \nabla n - q \mu_n n \nabla \psi + q n D_n \nabla T_n \quad (6)$$

$$\mathbf{S}_n = -K_n \nabla T_n - \left(\frac{k \delta_n}{q} \right) \mathbf{J}_n T_n \quad (7)$$

$$\nabla \cdot \mathbf{S}_p = \frac{1}{q} \mathbf{J}_p \cdot \mathbf{E} - W_p - \frac{3k}{2} \frac{\partial}{\partial t} \lambda_p p T_p \quad (8)$$

$$\mathbf{J}_p = q D_p \nabla p - q \mu_p p \nabla \psi + q p D_p \nabla T_p \quad (9)$$

$$\mathbf{S}_p = -K_p \nabla T_p - \left(\frac{k \delta_p}{q} \right) \mathbf{J}_p T_p \quad (10)$$

where:

S_n is the electron energy flux density

S_p is the holes energy flux density

W_n is the energy density loss for electrons

W_p is the energy density loss for holes
 T_n is the temperature of electrons
 T_p is the temperature of holes
 k is the Boltzmann constant
 λ is a constant related to the Fermi or Boltzmann statistics
 D_n is the thermal diffusivity for electrons
 D_p is the thermal diffusivity for holes
 K_n is the thermal conductivity for electrons
 K_p is the thermal conductivity for holes

The thermal diffusivities of electrons and holes derive from the frictional interaction of carriers with lattice and among themselves. Carriers are accelerated by the electric field but loose momentum due to scattering processes, including phonon, carriers and impurity scattering, surface and material imperfections. This effect is parameterized with a carrier mobility parameter, which is function of the electric field, lattice temperature and doping concentration and defines the carriers thermal diffusivity. In the low electric field regions of the detection structure the relation between mobility and carriers concentration is included in the model through an experimental look-up table. When the electric field magnitude increases, the mobility depends on he strength of the electric field parallel to the current flow. Such dependence is parameterised using the Caughey and Thomas expression [21].

The energy density losses W_{np} are defined by the interaction of carriers with the lattice . As mentioned before the leading phenomena in the description of the carriers scattering physics in the CMOS Silicon Photomultiplier are the impact ionization and the lattice and Auger recombination. It is possible to write the energy losses as:

$$W_n = \frac{3}{2}n \frac{k(T_n - T_L)}{\tau_n} \lambda_n + \frac{3}{2}kT_n \lambda_n R + E_g (G_n - R_n^A) \quad (11)$$

$$W_p = \frac{3}{2}n \frac{k(T_p - T_L)}{\tau_p} \lambda_p + \frac{3}{2}kT_p \lambda_p R + E_g (G_p - R_p^A) \quad (12)$$

where:

R^A is the Auger recombination rate
 T_L is the lattice temperature
 τ_n is the relaxation time for electrons
 τ_p is the relaxation time for holes
 E_g is the band-gap energy

The relaxation times are also important parameters in the modelling of the CMOS SiPM detection structure. We use the approximation $\tau_n \approx \tau_p \approx 1$ ps, which is retrieved in accordance with the experimental conditions.

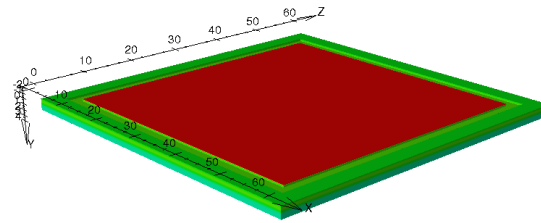
In the heavy doped region the decreased bandgap separation is included by lowering the conduction band level by the same amount as the valence band is raised. The separation between valence and conduction band in this regime is modelled according to the experimental results and theoretical studies in [22].

3.2 Definition of the modelling task

The CMOS Silicon photomultiplier is obtained using only standard CMOS processes. Hence the standard simulation framework SILVACO may be used for a realistic and precise determination of the features of the sensor [23]. The task is solved on a 3D domain with size $60 \times 60 \times 5 \mu\text{m}^3$.

We report in this section an illustrative example of a typically simulated structure consisting of a p^+/n SiPM obtained on a n-epitaxial layer. The guard ring structure is formed using STI. The example of the 3D domain is shown on Fig. 4.

Fig. 4 Example of simulated 3D CMOS Silicon Photomultiplier detection structure. In red the heavily doped p-region, in green the n-well. Around the p-region the STI are formed. The STI volume is invisible to simplify its identification in the 3D plot.



An interesting feature of the design of CMOS SiPM on a standard CMOS technology fab is that often the manufacturer does not provide a full access to the technology parameters in use. This happens in particular if the production and the R&D is based on Multi Project Wafer. It is hence a challenge for the modelling to identify the best profile fitting with the used technology and with the reduced set of technology information.

The cross-sectional view is shown on Fig. 5 and the profile at $x = 30 \mu\text{m}$ is shown on Fig. 6. The details of the doping profile are visible. The red volume corresponds to the heavily doped p-region. The green volume is the light-doped n-region. The doping profiles are extracted in this example from a direct measurement of a manufactured sample.

The doping concentration of the n-epitaxial region is about 10^{15} cm^{-3} . The n-well doping ranges from 10^{17} cm^{-3} in the space charge region to about $3 \times 10^{17} \text{ cm}^{-3}$ at a depth of $0.41 \mu\text{m}$. The p^+ doping peaks at $3 \times 10^{20} \text{ cm}^{-3}$ at a depth of $0.1 \mu\text{m}$. The junction is at a depth of 142 nm .

Around the junction STI is formed and filled with SiO_2 . The width and depth of STI are respectively $0.5 \mu\text{m}$ and $0.4 \mu\text{m}$, following the indications of the standard CMOS facility.

The computational domain is described by a tetrahedral mesh defined with an adaptive method in correspondence with the initial doping profile. The number of nodes is 40000000, the maximal allowed by SILVACO. The smaller mesh size is $0.1 \mu\text{m}$. This selection allows for a robust and convergent solution of the numerical problem. We verified that the numerical error in the estimation of the currents is in this case less than 3 %.

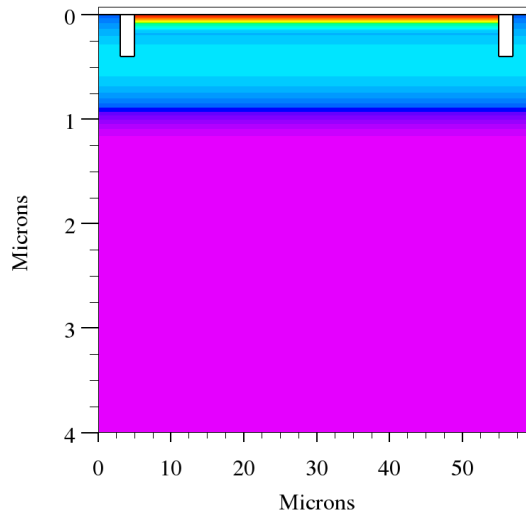


Fig. 5 cross-sectional view of the 3D CMOS Silicon Photomultiplier structure. The total concentration as well as the STI are visible (Colored version online).

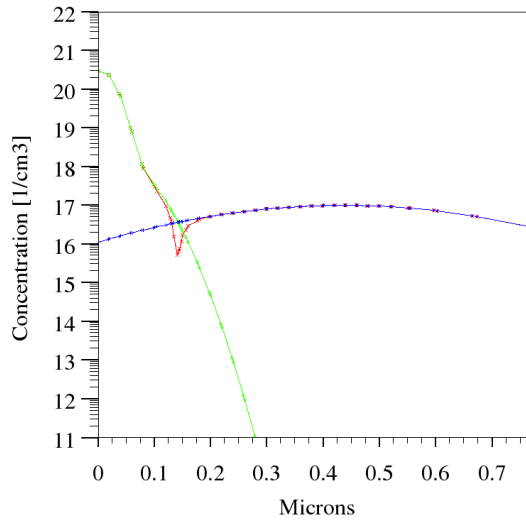


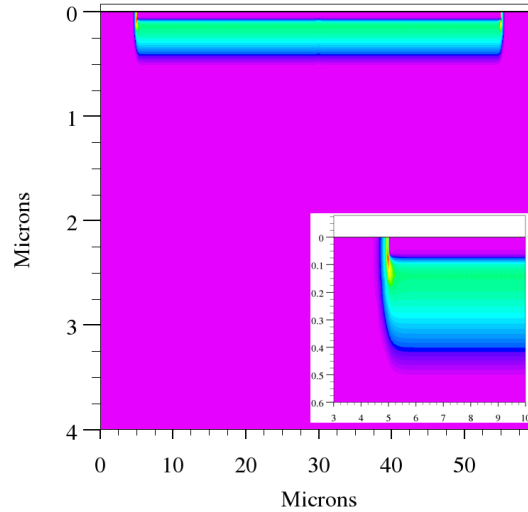
Fig. 6 Doping profile of the 3D CMOS Silicon Photomultiplier structure at $x = 30 \mu\text{m}$. The doping structure as well as the STI are visible. The width range is restricted to $0.8 \mu\text{m}$ for better visualization of the concentration profile. In green the free holes concentration, in blue the free electrons concentration, in red the net concentration.

3.3 Analysis of the electric field

A critical feature in the design of the CMOS SiPM is the possibility to obtain a uniform avalanche-breakdown mode along the sensitive area of the sensor. The condition is set by Eq. 4, which states that the ionization coefficients of the carriers and the corresponding current densities should be approximately constant along the

junction defining the sensitive area of the device. As these quantities depend on the electric field, Eq. 1 relates them ultimately to the geometry, size and doping of the detection structure. In particular it is enough to calculate the electric field satisfying the breakdown condition and to verify that the electric field is constant along the active area of the sensor.

Fig. 7 Electric field profile of a SiPM detection structure without guard rings at 0.1 V above breakdown. At the bottom of the figure the zoomed area of the junction corner is visualized. The electric field strength at the borders of the junction is higher. It causes a local breakdown deteriorating the overall performance of the sensor (Colored version online).



As an example, we show on Fig. 7 the electric field profile of a p/n structure designed without any protection of the borders of the heavily doped p-region (guard rings) at 0.1 V above breakdown. We observe that the electric field is constant along the sensitive area of the sensor, with a peak value of approximately 4.6×10^5 V/cm. However at the corners of the junction the electric field rises abruptly of one order of magnitude. This effect contributes to the local breakdown condition and deteriorates the performance of the sensor.

As stated before, the CMOS technology offers few possibilities of avoiding the local breakdown problem using only the available standard processes. The mathematical modelling is in this respect a powerful analysis and planning tool, as it gives an insight of the electric field of the structure, which is not experimentally observable. This information plays a central role in the correct design and is of guidance for the choice of the technological parameters.

We first analyse the possibility offered by the shallow trench isolation. The electric field corresponding to the detection structure analysed in Fig. 4 is shown on Fig. 8. The cross-sectional view of the electric field is shown on Fig. 9. The electric field is constant along the sensitive area of the detection structure. In comparison with Fig. 7, the electric field does not exhibit localized hot regions at the edges of the structure, due to the presence of the STI. The electric field has a peak value of

approximately 4.6×10^5 V/cm at a depth of 142 nm, defining the junction depth. The total width of the structure is defined by the shape of the electric field as approximately $420 \mu\text{m}$.

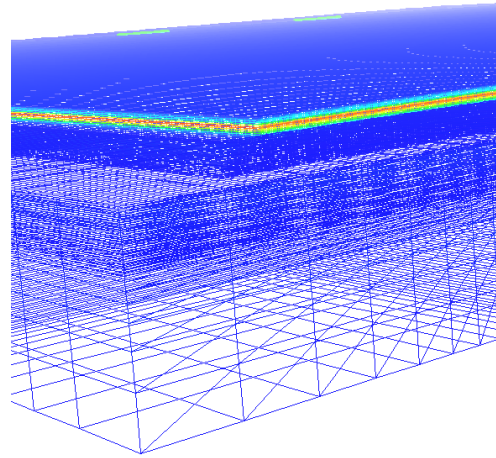


Fig. 8 Electric field of the SiPM detection structure shown on Fig. 4 at 0.1 V above breakdown. The electric field is constant along the sensitive area of the detector.

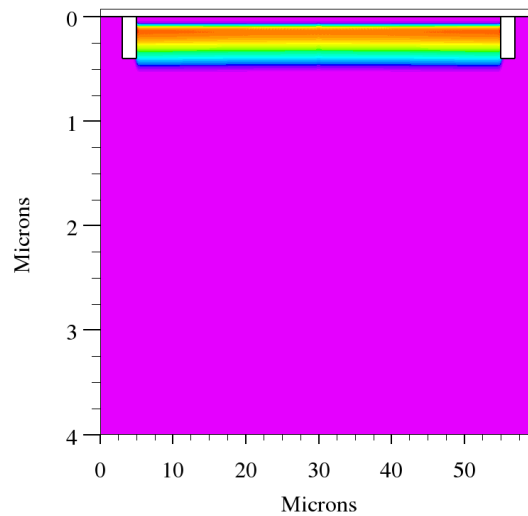


Fig. 9 2D electric field cross-sectional view of the SiPM detection structure shown on Fig. 4 at 0.1 V above breakdown. The electric field is constant along the sensitive area of the detector. (Colored version online)

Another possibility is offered by the virtual guard ring option. The cross-sectional view of the doping profile of such modelled structure is shown on Fig. 10. The doping concentration of the n-epitaxial region is about 10^{15} cm^{-3} . The n-well doping

ranges from 10^{17} cm^{-3} in the space charge region to about $3 \times 10^{17} \text{ cm}^{-3}$ at a depth of $0.41 \mu\text{m}$. The p^+ doping peaks at $3 \times 10^{20} \text{ cm}^{-3}$ at a depth of $0.1 \mu\text{m}$. The p^+ doping extends $1 \mu\text{m}$ longer on all sides of the sensitive area. The junction is at a depth of 142 nm . In addition, along the sides of the junction a p-well doped area with width $1 \mu\text{m}$ and with concentration ranging from 10^{17} cm^{-3} to about $3 \times 10^{17} \text{ cm}^{-3}$ at a depth of $0.41 \mu\text{m}$ is present.

The electric field cross-sectional view is shown respectively on Fig. 11. The electric field is constant along the sensitive area of the detector. The electric field has a peak value of approximately $4.6 \times 10^5 \text{ V/cm}$ at a depth of 142 nm , defining the junction depth. The total width of the structure is defined by the shape of the electric field as approximately $420 \mu\text{m}$. We observe that the virtual guard ring structure preserves the condition of the electric field at the edges of the junction, avoiding the occurrence of local breakdown.

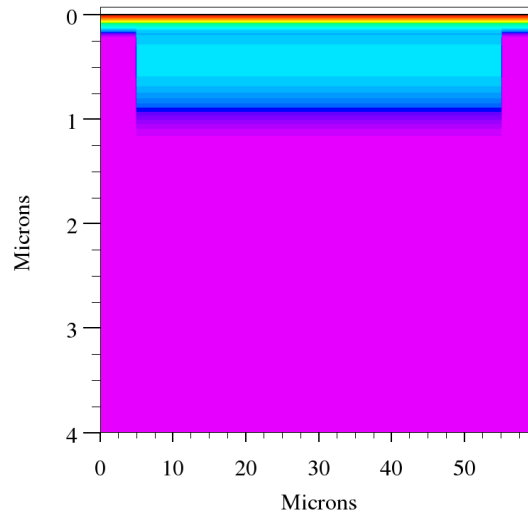


Fig. 10 Cross-sectional view of the total concentration of the SiPM detection structure with virtual guard rings. The electric field is constant along the sensitive area of the detector. (Colored version online)

3.4 The study of the current-voltage characteristics

The experimental observables of the mathematical model consist of quantities which can be measured with precision using dedicated measurement systems. The set of measurements includes the dependence of the current of the detection structure corresponding with the applied bias.

The calculated current voltage characteristics of the CMOS SiPM detection structure with STI guard rings is shown on Fig. 12. As an example, in this case,

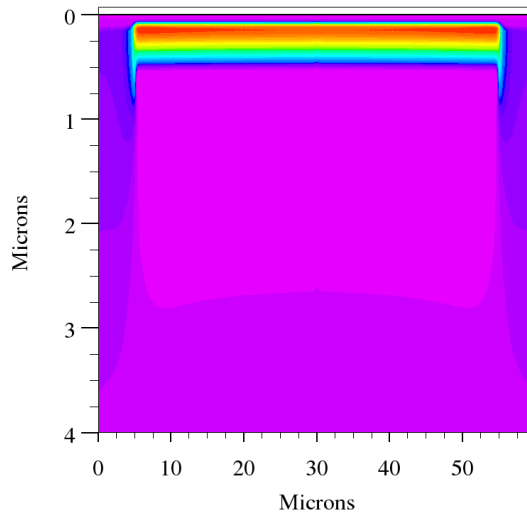


Fig. 11 Electric field cross-sectional view of the SiPM detection structure with virtual guard rings at 0.1 V above breakdown. (Colored version online)

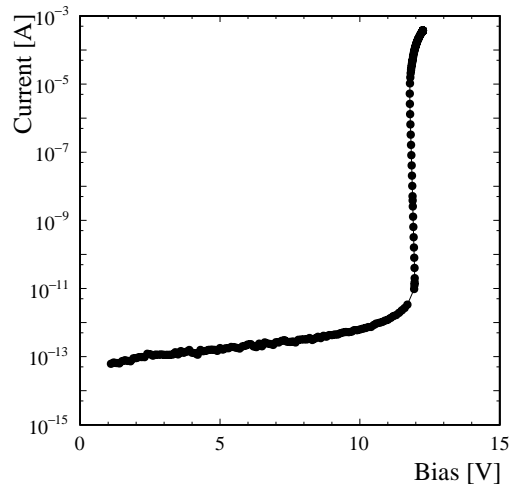


Fig. 12 Calculated current-Voltage characteristics of a CMOS SiPM detection structure with STI guard rings.

the open circles correspond to a calculation in which the generation rate through impact ionisation is artificially set to zero. The corresponding curve is hence only sensitive to thermal noise and to the leakage current of the device. The filled circles correspond to the calculation using the full model, including impact ionization. The curve follows the leakage current behaviour up to a level of approximately 1 pA. After that the electric field strength begins to be sizeable and the impact ionization process let the current increase exponentially and abruptly up to a level of approx-

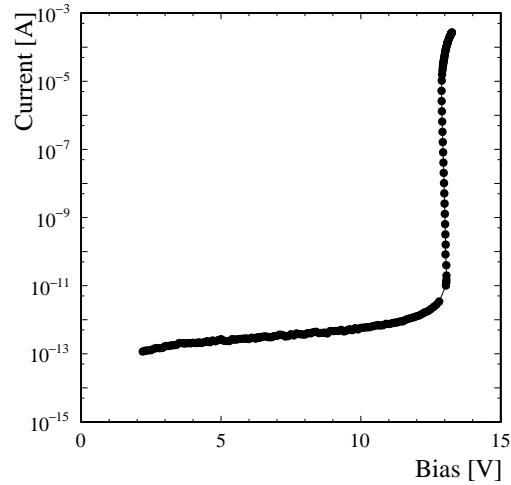


Fig. 13 Calculated current-Voltage characteristics of a CMOS SIPM detection structure with virtual guard rings.

imately $10 \mu\text{A}$, at which the external quenching resistor begins limiting the current of the device. The expected breakdown voltage of the device is approximately 12 V.

The calculated current voltage characteristics of the CMOS SiPM detection structure with virtual guard rings is shown on Fig. 13. The curve follows the leakage current behaviour up to a level of approximately 1 pA. After that the electric field strength begins to be sizeable and the impact ionization process let the current increase exponentially and abruptly up to a level of approximately $10 \mu\text{A}$, at which the external quenching resistor begins limiting the current of the device. The expected breakdown voltage of the device is approximately 13 V. We observe that the expected level of leakage current is slightly higher than in the STI guard rings case. The higher breakdown voltage is consistent with the expectation that the electric field with virtual guard rings increases less abruptly and is more regular, in particular in the vicinity of the edges.

4 Experimental results

To investigate the possibilities within the standard CMOS processes in Multi Project Wafer, we produce detection structures with the two different kinds of guard rings proposed in Fig 1 and modelled in the previous section. The production is performed in the 180 nm BCDLite IC MPW node at Global Foundries. We choose the process with n-type epitaxial layer, on which the photo-detection structures based on p^+/n junctions are formed. The active area of the junction is $50 \times 50 \mu\text{m}^2$. We do not optimize the optical window above the active area with anti reflective coating. However, we minimize the thickness of the SiO_2 covering by using the minimal number

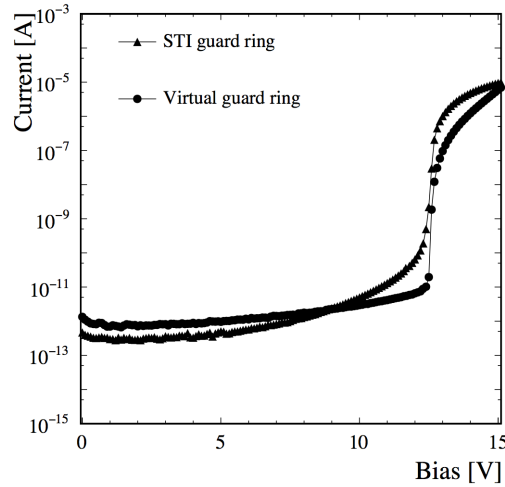


Fig. 14 Measured current-voltage characteristics of the SiPM structures. The circles correspond to STI guard ring, the triangles to the virtual guard ring structures.

of three metal layer offered in this technology. In fact, although there is clearly no metal above the active area of the sensor, in CMOS MPW the SiO_2 isolation layers between metal layers are deposited indistinctly on the whole area of the chip.

The structures are operated in breakdown mode and a quenching element is needed in order to stop the avalanche. We choose to implement a passive quenching element consisting of a resistor integrated around the sensitive cell. The used CMOS MPW line includes High Resistive Polysilicon as a standard process. We design a quenching element of $250 \text{ k}\Omega$ with a sheet resistivity of $2 \text{ k}\Omega$ and a minimal width of $0.5 \mu\text{m}$. We produced a series of test resistors on the same wafer of the detection structures and we measured the spread of the resistor values to be 3 % in this technology. This result is compatible with the requirements of the SiPM design.

4.1 Current-voltage characteristics

The current-voltage characteristics of the two produced structures is shown on Fig. 14. The structure with STI guard ring exhibits a slightly lower breakdown voltage (about 12.5 V) with respect to the structure with virtual guard ring (about 13.2 V). In comparison with the modelling results, the mathematical model and the experimental results are in good agreement regarding the prediction of the breakdown voltage.

The dark current level is significantly different between the two structures. The virtual guard ring structure exhibits a dark current below a few picoamperes before avalanche breakdown. At breakdown the current rises abruptly up to a few nanoamperes. After breakdown it gets limited by the quenching resistor and rises

linearly. The STI guard ring structure exhibits a larger dark current, reaching a few nanoamperes already before breakdown and a few microamperes at breakdown, before getting limited by the quenching resistor. The additional dark current obtained in STI guard rings is related to defect generation during the trench etch process. As we already tested in other CMOS technology facilities, this effect is by far limiting the possibility of the use of STI guard rings in Multi Project Wafer [13]. The production of devices in MPW follows the standard processes and it is not possible a user-oriented optimization. As clear from a direct comparison of Fig. 14 and Fig. 12-13, the effect of the defect generation in the trenches process is not included in the mathematical model and further improvements are needed in order to predict the deterioration of the current properties using the STI technology in the production of the sensor.

Thermal e/h pairs created in the sensitive area of the SiPM generate an output signal which is not distinguishable from a single detected photon. Such effect is called dark rate. We measure the amplitude of dark rate pulses in the two proposed photon-detection structures by biasing the structure at a voltage 0.2 V above the breakdown and observing the output signal with a 4 GHz bandwidth oscilloscope after an high frequency $18\times$ voltage amplification stage. The virtual guard ring structure exhibits a dark rate signal with amplitude of approximately 30 mV, well above the 2 mV noise level of the experimental setup. The dark rate measured for signals whose amplitude is above the 0.5 single photon threshold (15 mV) is approximately 3 KHz. As the output signal corresponding to the single photon is equivalent to the dark rate pulse, this result demonstrates that the virtual guard ring structure is capable to provide a sizable signal in correspondence of a photon detected. On the contrary, the STI guard ring structure did not provide any dark rate signal in the same experimental conditions. This result reflects the large leakage observed in the current voltage characteristics of such structure.

4.2 Optical and Gain characteristics

Following the results of the single cell performances, we produce on the same MPW a prototype of SiPM consisting of an array of photo-detection cells with virtual guard rings. For the photodetector characterization a 850 nm LED light source and a circular lensed fiber with 10 μm spot size was used for injecting light into the SiPM.

The dc characterization is performed on wafer. The LED light source is operated in continuous mode. The current-voltage characteristics of the SiPM prototype at dark conditions and with light are shown on Fig. 15. The dependence of the current versus voltage is following the behavior of the single cell and there is no significant deviations from the expectations. The level of the current-voltage curve under light exposure shows a visible increase, due to the current generated by photon detection. Although the optical window of this prototype is not optimized the prototype exhibit a sizable photon detection efficiency.

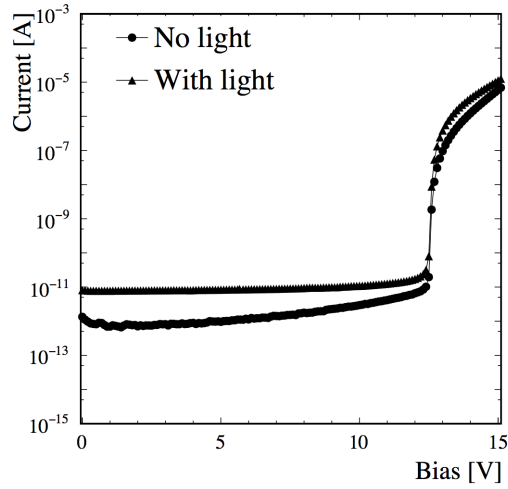


Fig. 15 Measured current-voltage characteristics of an array of 5×5 SiPM structures with virtual guard rings. The crosses correspond to dark condition, the triangles to illumination condition.

The photodetector characterization is performed with packaged samples of the prototypes. The LED light source is pulsed with a pulse width of 10 ns. The SiPM output signal is amplified with a high frequency $18\times$ voltage amplifier and integrated with the CAEN V1180 QDC within an integration gate of 150 ns.

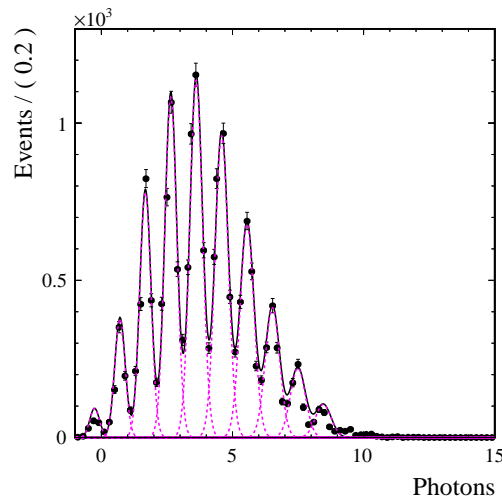


Fig. 16 Spectrum of the low photon flux detected by a SiPM prototype.

Fig. 16 shows the spectrum of the signal corresponding to the used low photon source. The histogram plots the distribution of the integrated sensor current for an

average detected flux of photons $\mu = 4$. Here the sensor is biased at 1 V above the breakdown voltage. The integrated current is shown in units of correspondent number of electrons. The histogram exhibits a series of peaks at etc. which we identify as induced by 0, 1, 2, 3 etc. photons.

The 0-photon peak corresponds to a period on which there is no photo-induced avalanche, only electric noise of the external circuit components. The black continuous thick line on Fig. 16 shows a fit to the data assuming a poissonian distribution of the incident LED light pulses. We fitted the spectrum with a sum of Gaussians, with area weighted according to a poissonian distribution, using a fitting technique explained in [13]. The peaks are assumed to be equally spaced. The spectrum is consistent with a poisson-distributed light and the histograms on Fig. 3 and Fig. 4 can be interpreted as a representation of a specific photon number state.

The fitted distance between the peaks is $G=(1.706 \pm 0.003) \times 10^6$ electrons. This distance represents the number of electrons produced during the avalanche process before the quenching occurs. In other words it is the intrinsic gain of the sensor. We observe that the intrinsic gain is high enough to separate the signal corresponding to the single photon detection from the electronic noise level. The possibility of observing the single photon spectrum on Fig. 16 depends strongly on the uniformity of the gain of each sensor microcell and is a proof of the high quality and reliability of the CMOS technology processes used in the fabrication.

5 Conclusions

The progress on the mass production of the conventional SiPMs is fully laying on the CMOS technology industrial facilities. Furthermore the overall future development of the new SiPM structures, as Digital Silicon Photomultipliers, Digital Silicon Photomultiplier imagers, Avalanche Pixel Structures for the detection of ionization particles is dependent on the CMOS technology. We have shown evidence that the main component - the photosensor - can be realized in the CMOS technology. Further developments will concentrate on the optimisation of the sensor performance, using the modern development in CMOS technology as 3D Inter Connection technology, which is very efficient and perspective for the sensor part. The future main effort will be focused on the development of the fully digital readout electronics and the additional powerful processing electronics on the chip. It will widely improve the overall performance and reliability of the SiPMs, as sensor for the low photon flux and widely increase the areas of applications [25].

References

1. H. Toshikaza, *Photomultiplier tubes, basics and applications*, (Hamamatsu Photonics K. K., Electron tube division, Japan, 2006)

2. M. Atac, J. Park, D. Cline, D. Chrisman, M. Petroff, E. Anderson, Nucl. Instrum. Methods. Phys. Res. A **314**, 56 (1992)
3. V. Saveliev, V. Golovin, Nucl. Instr. Meth. A, **442**, 223 (2000)
4. V. Golovin, V. Saveliev, Nucl. Instr. Meth. A, **518**, 560 (2004)
5. A. G. Chynoweth, K.G. McKay, Phys. Rev., **102**, 369 (1956)
6. V. Saveliev, *Quantum Detector Arrays* (US Patent US 7,825,384, 2010)
7. N. D'Ascenzo, V. Saveliev, Q. Xie, L. Wang, in *Optoelectronics - Materials and devices* ed. by S. Pyshkin and J. Ballato (Intech, 2015)
8. N. D'Ascenzo, P. Marrocchesi, C. S. Moon, F. Morsani, L. Ratti, V. Saveliev, A. Savoy-Navarro, Q. Xie, J. Instrum. ,**9** C03027
9. N. D'Ascenzo, V. Saveliev, in *Photodetectors* ed. by S. Pyshkin and J. Ballato (Intech, 2015)
10. D.J. Herbert, V. Saveliev, N. Belcari, N. D'Ascenzo, A. Del Guerra, A. Golovin, IEEE Trans. Nucl. Sci. **53**, 389 (2006)
11. V. Saveliev, in *Advances Optical and Photonic Devices* ed. by W. Shi (Intech, 2012)
12. N. D'Ascenzo, V. Saveliev in *Photodetectors* ed. by Jin-Wei Shi (Intech, 2012)
13. N. D'Ascenzo, V. Saveliev, L. Wang, Q. Xie, Journ. Instrum. **10** C08017 (2015)
14. M. Lee, H. Rucker, W. Choi, IEEE Electr. Dev. Lett., **33**, 80 (2012)
15. M. Lee, H. Rucker, W. Choi, IEEE Electr. Dev. Lett., **37**, 60 (2016)
16. N. Izhaky, M.T. Morse, S. Kohel, O. Cohen, D. Rubin, A. Barkai, G. Sarid, R. Cohen, M.J. Paniccia, IEEE J. Sel. Topics Quantum Electronic, **12**, 1688 (2006)
17. W. Sul and J. Oh and C. Lee and G. Cho and W. Lee and S. Kim and J. Rhee, IEEE Electr. Dev. Lett. **31** 41 (2010)
18. K. Katayama, T. Toyabe, IEDM technical digest, 135 (1989)
19. W. Shockley, W. T. Read, Phys. Rev. **87**, 835 (1952)
20. J. G. Fossum, R.P. Mertens, D.S. Lee, J.F. Nijs, Solid State Electronics **26**, 569 (1983)
21. D. M. Caughey, R. E. Thomas, Proc. IEEE **55**, 2192 (1967)
22. J.W. Slotboom and H.C. De Graaf, Solid State Electronics **19**, 857 (1976)
23. Silvaco, www.silvaco.com
24. N. D'Ascenzo, V. Saveliev, Q. Xie, Proceedings of the 4th International Conference on Photonics, Optics and Laser Technology (PHOTOPTICS 2016), 215.
25. N. D'Ascenzo, V. Saveliev, Nucl. Instr. Meth. A, **695**, 265 (2012)